Theor Chem Account (2007) 118:485–493
DOI 10.1007/s00214-007-0369-4

REGULAR ARTICLE

He photoionization: β_N and σ_N below $N=5$ and 6 thresholds

Dipole asymmetry parameters below $N=6$ threshold are computed for the first time by means of a B-spline based K-matrix method

Luca Argenti · Roberto Moccia

Received: 15 December 2006 / Accepted: 26 February 2007 / Published online: 23 June 2007

Abstract In this paper we use the results of a K-matrix method calculation to evaluate the ionization spectrum of He between the $N = 4$ and 6 parent ion thresholds. Partial dipole asymmetry parameters β_N below $N = 6$ threshold have been computed for the first time and compared to the available preliminary experimental findings by Jiang and Püttner [http://www.diss.fu-berlin.de/2006/269].

1 Introduction

Since the pioneering experiments of Madden and Coddling [1] and the theoretical study of Cooper et al. [2] the complexity of the ionization spectrum of He has continuously attracted the attention of experimentalists and theoreticians prompting several advances in theory and experiments.

Nowadays, thanks to the improvements in the experimental equipments and computational methods and capabilities, the experimental knowledge and the theoretical understanding of He spectrum has increased hugely. The experimental data cover an energy range up to the $N = 9$ threshold [3,4] with a resolution reaching in some case a few meV while theory, through a variety of approaches, is able to account with satisfactory accuracy for most of the available data [5,6].

The theoretical literature reports various attempts to label the doubly excited autoionizing states, which dominate the spectrum, by additional "almost conserved" quantum numbers.

Three major classification schemes are commonly in use: parabolic $[N_1 N_2 m]_n^A$, molecular $(n_\lambda, n_\mu, m)_n$, and Herrick's ${}_N(K,T)_n^{A'}$. In the present paper the parabolic notation will be used throughout. Herrick's classification scheme ${}_N(K,T)_n^{A'}$ is almost a shorthand notation for the parabolic scheme with $N = N_1 + N_2 + |m| + 1$, $K = N_2 - N_1$ and $T = |m|$. $A' = \pm 1, 0$ specifies the series invariant antinodal/nodal/non nodal character of the adiabatic hyperspherical wavefunction at $r_1 = r_2$. When $A' \neq 0$ then $A' = A$ (see [7] and references therein for further details).

The classification schemes cited thus far account quite accurately for spectrum details in the lower energy region but progressively loose validity at higher energies because of an increasing number of intruder states which act as perturbers on regular multiplet resonant series. This type of occurrences becomes more and more pronounced at higher energies and, as studied by Püttner et al. [8], the NNS of the doubly excited states, obtained experimentally and theoretically, reveals a clear transition toward quantum chaos.

In a previous paper [9] we employed the reaction K-matrix implemented using L^2 elementary basis functions (B-splines, for radial dependence, times spherical harmonics) to accurately study the energy region between the $N = 3$ and 4 thresholds analyzing in great detail the effect of the first ${}^1\mathrm{P}^o$ intruder state, $[031]_5^+$, upon the resonance series.

In this paper the energy region below $N = 5$ and 6 thresholds is studied by the same approach, obtaining positions and width of resonances, total cross section, partial cross sections σ_N and dipole asymmetry parameters β_N. The positive comparison with all the most accurate experimental and theoretical data available below $N = 5$, and with total and partial cross section data below $N = 6$, confirm the reliability of the method. Asymmetry parameters β_N below $N = 6$ are, as

Dedicated to Prof. Serafin Fraga.

L. Argenti
Dipartimento di Chimica Applicata e Scienza dei Materiali (DICASM), Università di Bologna, Via Saragozza 8, 40136 Bologna, Italy

R. Moccia (✉)
IPCF, CNR, Via G. Moruzzi 1, 56100 Pisa, Italy
e-mail: roberto.moccia@ipcf.cnr.it

far as we know, reported for the first time and are compared to the available preliminary experimental data of Jiang [10].

2 Method

The L^2-K matrix method has already been applied successfully to several problems in atomic and molecular physics [11–17]. Since this method, as implemented here, was described in a previous publication [9] here only a very brief summary will be given.

The stationary wave function $\phi^{\mathcal{P}}_{\alpha E}$ in the continuum is expressed, as in the Close Coupling approach, as a linear combination of partial-wave channels (PWCs) $\phi_{\beta E}$ plus localized functions ϕ_j collected in a set labeled localized channel (LC).

Greek indices collect all the quantum numbers, besides energy, needed to fully characterize a state. For each channel, the PWC functions are expressed as antisymmetrized products of an assigned ion target state times very diffuse orbitals, while the LC basis comprises antisymmetrized products of localized orbitals. These last orbitals are also used to build the target states.

Each PWC basis, as well as the LC basis are transformed in order to give, separately, diagonal representation of the Hamiltonian. Thus the stationary wave function in the continuum, employing the usual definition of the off shell reaction scattering matrix K, may be expressed as

$$\psi^{\mathcal{P}}_{\alpha E} = \phi_{\alpha E} + \sum_{\gamma} \sum\!\!\!\!\!\!\int \mathrm{d}\epsilon \phi_{\gamma\epsilon} \frac{\mathcal{P}}{E-\epsilon} \mathsf{K}_{\gamma\epsilon,\alpha E} \tag{1}$$

where the index α indicates an open channel at the energy E while the index γ runs upon all available channels (open and closed) including the LC.

With the requirement $\langle \phi_{\beta\epsilon} | E - H | \psi^{\mathcal{P}}_{\alpha E} \rangle = 0 \ \forall \beta, \epsilon$ the following "off-shell" K matrix determining equation is obtained

$$\mathsf{K}_{\beta E',\alpha E} - \sum_{\gamma\neq\beta} \sum\!\!\!\!\!\!\int \mathrm{d}\epsilon \langle \phi_{\beta E'} | H - E | \phi_{\gamma\epsilon} \rangle \frac{\mathcal{P}}{E-\epsilon} \mathsf{K}_{\gamma\epsilon,\alpha E} = \langle \phi_{\beta E'} | H - E | \phi_{\alpha E} \rangle \tag{2}$$

In our method PWC basis functions are projected on an L^2 basis. As a consequence Eq. (2) is reduced to a finite set of discrete energy grids yielded by the diagonalization of each PWC channel. It is therefore essential that energy grids are thick enough to allow for a reliable interpolation of matrix elements at arbitrary energies.

To achieve satisfactory results the elementary basis functions must satisfy three main requirements:

(i) to be able to describe the localized ionic target states and the localized electronic distribution in order to account for the short range correlation between the target electrons and the photo-electron,
(ii) to mimic the behavior of the photo-electron wave in a large extension of space where non monopolar interaction terms may still be influent,
(iii) to account adequately for the Rydberg series associated to the several states of the target taken into account.

The elementary basis functions employed in the present paper are radial-dependent B-splines times spherical harmonics. The above requisites are accomplished by using three different sets of B-splines: the first one for the localized basis, uses knots up to $\simeq 70$ au, whose spacing increases exponentially with r with a further thickening close to the nucleus; the second one coincide with the first one for $r \leq 1.5$ au and is augmented by a series of equally spaced knots up to a few hundreds au; the third one comprises the second one plus a series of more spaced knots up to a few thousands au. The first set is actually a subset of the second. Because of the way B-splines are defined, the corresponding function spaces are both exact subspaces of that defined on the most large grid.

To avoid redundancy problems which arise in a two electron space builded as direct sum of PWC plus LC channels some care is required. As detailed at length in [9] it is possible to rearrange the basis in order to eliminate the redundancies.

At each energy, with n open channels, n linearly independent coupled-channel functions $\psi^{\mathcal{P}}_{\alpha E}$ are obtained. Ordinary scattering solutions $\boldsymbol{\psi}^{\pm}_{E} = (\psi^{\pm}_{1E}, \ldots, \psi^{\pm}_{nE})$ are obtained through the transformation

$$\boldsymbol{\psi}^{\pm}_{E} = \boldsymbol{\psi}^{\mathcal{P}}_{E} [\mathbf{1} \pm i\pi \mathbf{K}(E)]^{-1}, \quad \langle \boldsymbol{\psi}^{\pm}_{E} | \boldsymbol{\psi}^{\pm}_{E'} \rangle = \delta(E - E')\, \mathbf{1}.$$

where $\mathbf{K}_{\alpha,\beta}(E) \equiv \mathbf{K}_{\alpha E,\beta E}$ is the on-shell reactance matrix. The scattering matrix is then

$$\langle \boldsymbol{\psi}^{-}_{E'} | \boldsymbol{\psi}^{+}_{E} \rangle = \delta(E - E') \mathbf{S}(E), \quad \mathbf{S}(E) = \frac{\mathbf{1} - i\pi \mathbf{K}(E)}{\mathbf{1} + i\pi \mathbf{K}(E)}. \tag{3}$$

The resonances are searched as poles of the scattering matrix $\mathbf{S}(E)$ in the lower complex energy half plane. The problem can be reduced to the search of poles of the $\mathbf{S}(E)$ determinant:

$$\det \mathbf{S}(E) = \exp\left\{ 2i \sum_{j}^{\text{open}} \varphi_j(E) \right\}$$

where the eigenphases $\varphi_j(E)$ are related to the real eigenvalues $\lambda_j(E)$ of $\mathsf{K}(E)$ matrix through
$\varphi_j(E) = -\arctan[\pi \lambda_j(E)]$.

The determinant is unimodular on the real axis and clearly have the same poles of $\mathbf{S}(E)$ which consequently appear as

well known Breit–Wigner phase factors:

$$e^{2i\varphi_j(E)} = \frac{E - E_j - i\Gamma_j/2}{E - E_j + i\Gamma_j/2},$$

$$\varphi_j = -\arctan\left[\frac{\Gamma_j}{2(E - E_j)}\right]$$

where E_j and Γ_j are respectively energy and width of the j-th resonance.

For a not too large energy interval comprising $N_{\rm res}$ resonances, $\det \mathbf{S}(E)$ may be written as product of a smooth background phase factor and $N_{\rm res}$ resonance phase factors. Thus, to find resonance positions, the sum of the eigenphases φ_j are fitted with a linear combination of arcotangent "step" functions plus a smooth polynomial background. This procedure has to be applied separately for each group of resonances. The fitting energy interval has to be small enough to reduce large variations of background phaseshift and must contain a limited number of resonances otherwise the minimization fitting procedure fails.

Figure 1 illustrates the fitting procedure. Total phaseshift, divided by π, around an isolated doubly excited states multiplet in $^1P^o$ symmetry below $N = 5$ threshold is reported as a function of energy together with its derivative (scaled to fit in the plot), which represents the density of states.

The fitting function (nine resonance terms plus a polynomial background of fourth degree) is superposed to the phase shift as a thicker line. Resonance parameters which result from the fitting procedures are reported in Table 1. The outer principal quantum number n of resonance classification is chosen to match with the convention of Rost et al. reference [7].

The multiplet series perturbed by intruder states eventually stabilizes in a periodic pattern (that is the derivative of total phaseshift with respect to the effective quantum number $n^* \equiv [2(E_{\rm thr} - E)]^{-1/2}$ converges to a periodic function of n^*), at least in electrostatic approximation where radiative decay and relativistic effects are ignored and all resonant series consequently converge to the same threshold.

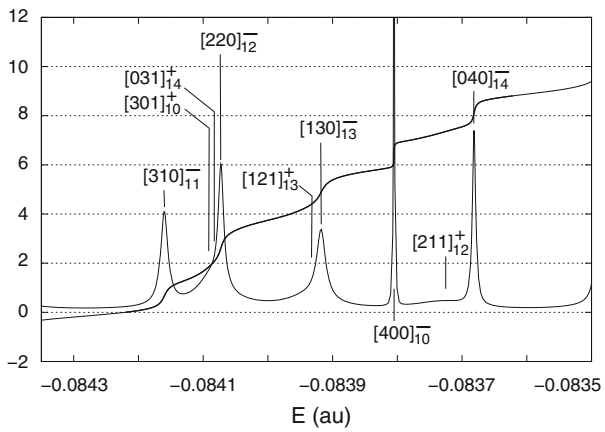

Fig. 1 Total phaseshift and state density for an isolated multiplet below $N = 5$ threshold

Table 1 Parameters of resonances in Fig. 1

$[N_1 N_2 m]^A$	E (au)	$\Gamma/2$ (au)
$[031]^{+}_{14}$	−0. 084 080	6.79[−5]
	−0. 084 092	6.29[−5][a]
$[121]^{+}_{13}$	−0. 083 935	4.19[−5]
	−0.083 966	5.68[−5][a]
$[211]^{+}_{12}$	−0. 083 729	5.76[−5]
	−0. 083 737	5.97[−5][a]
$[301]^{+}_{10}$	−0. 084 087	2.38[−5]
	−0. 084 103	2.48[−5][a]
$[040]^{-}_{14}$	−0. 083 682	2.76[−6]
	−0. 083 678	2.87[−6][a]
$[130]^{-}_{13}$	−0. 083 918	7.79[−6]
	−0. 083 919	7.60[−6][a]
$[220]^{-}_{12}$	−0. 084 073	4.76[−6]
	−0. 084 079	5.84[−6][a]
$[310]^{-}_{11}$	−0.084 160	6.37[−6]
	−0. 084 169	5.77[−6][a]
$[400]^{-}_{10}$	−0. 083 805	3.77[−7]
	−0. 083 820	3.21[−7][a]

[a] Rost et al. (1997) [7]

Huge resonances with widths comparable to or larger than intermultiplet distance may be missed because they cannot be distinguished from a polynomial background in a small interval. A technique to circumvent this is to subtract the narrowest fitted resonances and to repeat the fitting procedure on the residual spectrum.

3 Results

All the calculations were carried out employing elementary basis functions with values of orbital angular momentum ℓ up to 6, obtaining $E(1^1S^e) = -2.903\,642\,673$ au for the energy of the ground state (accurate electrostatic limit $-2.903\,724\,377$ au [18]) in good agreement with the estimated limit for $\ell_{\rm max} = 6$ of $-2.903\,643\,88$ au [19]. The Rydberg constant used for the binary system $^4He^+ - e^-$ is $R_{^4He^+} = \frac{M_{^4He^+}}{M_{^4He}} R_h = 13.603828(12)\,\text{eV}$.

Energy scale is given as the experimental first ionization potential of helium plus the theoretical excitation energy with respect to the ground state of He^+.

Since parent He^+ states are built in a finite size box, energies of states with different angular momenta differ by tiny amounts. $N = 5$ threshold energies range from $-0.\,079\,999\,942$ au for $5s$ level to $-0.079\,999\,999$ au for $5g$

level. $N = 6$ threshold energies range from $-0.055\,555\,235$ au for $6s$ level to $-0.055\,555\,553$ au for $6h$ level. An average over all angular momenta is taken as reference: $E^5_{\rm av} = -0.079\,999\,977$ au, $E^6_{\rm av} = -0.055\,555\,410$ au. These discrepancies are much smaller than the estimated errors upon the calculated energies of the two electron states.

3.1 Energy interval between $N = 4$ and $N = 5$ thresholds

Many experiments have been devoted to the energy interval below $N = 5$ threshold to find total cross section [20–23], partial cross sections [23–28], total [25] and partial [23,27] dipole asymmetry parameters. In some cases, resonance parameters have been extracted from experimental results [21,22]. In the following we will refer mainly to the measurements by Domke et al. [22] with a photon beam of 5.4 meV FWHM for the total cross section, to the measurements by Menzel et al. [23] with 12 meV FWHM resolution for the β_N and σ_N, and to the more recent σ_N measurements by Jiang et al. [28] obtained with a resolution of 6 meV FWHM.

On the theoretical side, a large number of techniques have been applied. Resonance parameters are generally determined by means of complex rotation. Here we will refer to the review by Rost et al. [7] for both doubly excited states classification schemes and comparison of resonance parameters. In the calculation of total and partial cross sections and asymmetry parameters, R-matrix method has been the favored one. The reader is particularly referred to the papers by Schneider et al. [6], by van der Hart and Greene [5], where a B-spline basis has been adopted, and to references cited therein.

Resonances. In Fig. 2 our theoretical results are compared with those by Rost et al. [7]. On the x axis the effective principal quantum number n^* is reported while on the y axis the reduced width $\bar{\Gamma} = \Gamma(n^*)^3$ on a log-scale is reported. There is an excellent agreement for $[211]^+$, $[301]^+$, $[130]^-$ and $[040]^-$ series which all display a regular behavior.

As it is well known, two intruder states formally belonging to two series converging to the higher $N = 6$ threshold fall in this energy interval, the $[041]^+_6$ state which causes the modulation of $[031]^+$ series, and the $[131]^+_6$ state, which causes the $[121]^+$ series quenching (see [7] for more details). Also for these two perturbed series there is still a fairly good agreement.

The $[220]^-$ and $[310]^-$ series differ slightly in our and in Rost treatment. In our calculations the two series come closer a couple of terms earlier than in Rost results but remain more separated in width, while those calculated by Rost yield almost indistinguishable doublets.

An inferior agreement is found in the narrowest $[400]^-$ series. Extremely narrow series are actually more difficult

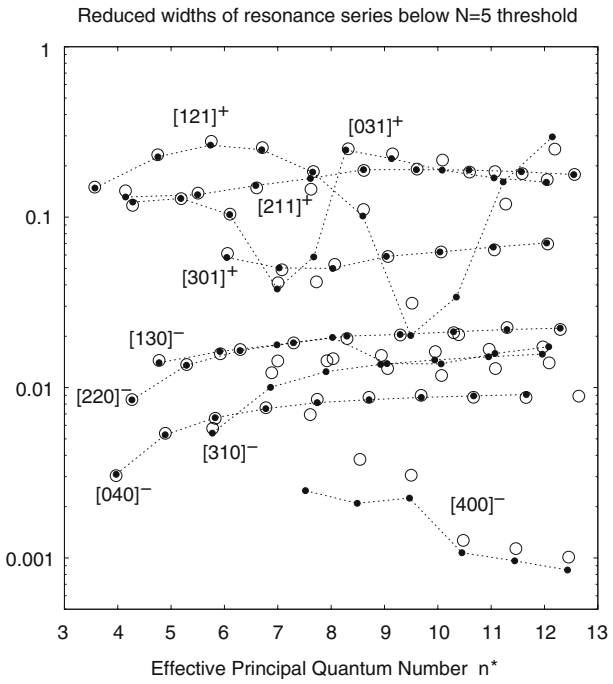

Fig. 2 Reduced width $\bar{\Gamma}$ *versus* n^*, the effective principal quantum number of the nine series in the $N = 4$–5 interval. *Filledcircle with dots* — Rost et al. [7]; *opencircle* — present results

to be determined numerically and absolute differences are actually much amplified in a logarithmic scale, so that at the moment we cannot conclude if these differences are due to a different representation of system dynamics or rather to the width determining algorithm.

Cross sections. The agreement of total and partial cross sections with experimental results is quite satisfactory. In Fig. 3 the total cross section convoluted with a gaussian profile with FWHM = 5.4 meV is presented. A linear background $\sigma_{\rm bg} = -(E - 76.4\,{\rm eV})0.025\,{\rm Mb/eV}$ has been subtracted for a ready comparison with total cross section measurements by Domke et al. [22]. The agreement among the three reported gauges, length, velocity and acceleration, is excellent. The tiny discrepancies, less than one part over thousand, are mainly due to the $N = 1$ partial cross section. For all other partial cross sections, the gauge agreement is even better (by an order of magnitude or so). Thus all other plots report only the velocity gauge.

In Fig. 4 the total cross section is compared with experimental data by Menzel et al. [23,27] scaled by a factor 1.048.

In Figs. 5, 6, 7 and 8 our theoretical partial cross sections have been compared with data by Menzel et al. [23,27] and by Jiang et al. [28]. Data by Jiang are on an arbitrary scale so a suitable factor has been applied. As in the case of total cross section, a scaling factor has been applied even to partial cross sections: 1.062 ($n = 1$), 0.905 ($n = 2$),

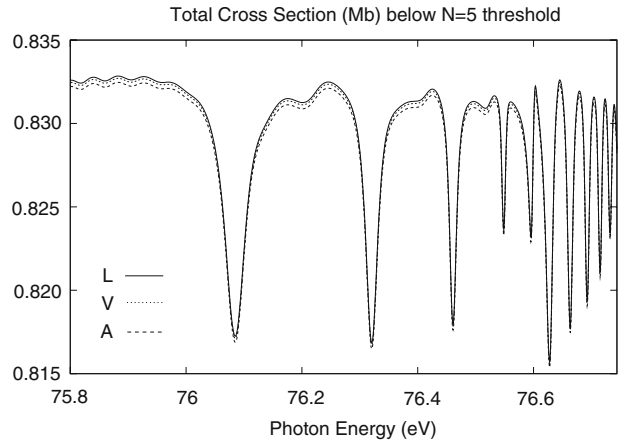

Fig. 3 Total cross section below $N = 5$ threshold where a linear background has been eliminated (see text for details)

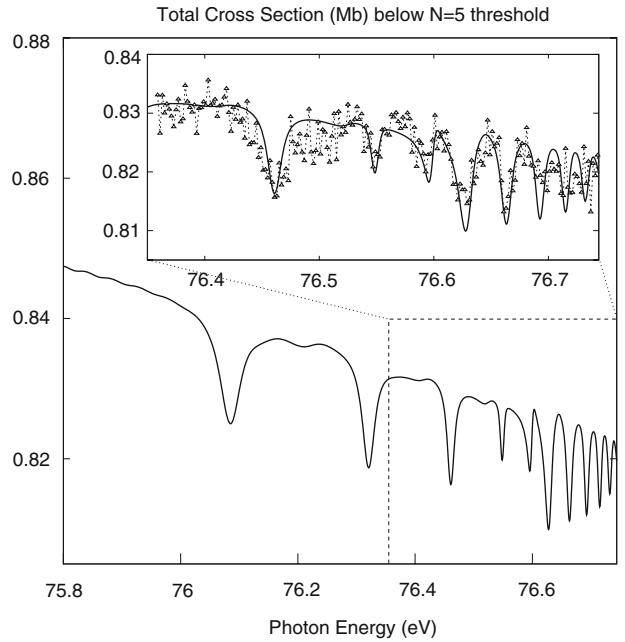

Fig. 4 Total cross sections below $N = 5$ threshold. In the *inset* enlargment, the present calculation (*continuous line*) is compared with measurements by Menzel et al. (*triangle*) [27]. Experimental results have been scaled by a factor 1.048

1.0 ($n = 3,\ 4$). It is interesting to observe that almost identical scaling factors (1.05 for σ_{tot}, 1.06 for σ_1, 0.915 for σ_2, 1.0 for $\sigma_{3,4}$) have been applied by the same authors in their original experimental/theoretical paper [23] in order to compare the experimental data with the calculated ones. In reporting the experimental data for $\sigma_{3,4}$, an energy shift of -3 and $+2$ meV has been applied to Jiang and Menzel data, respectively. All partial cross sections have been convoluted with a FWHM = 6 meV gaussian. All experimental and theoretical data agree very well. Menzel data have a much smaller dispersion than those by Jiang, but the energy resolution is

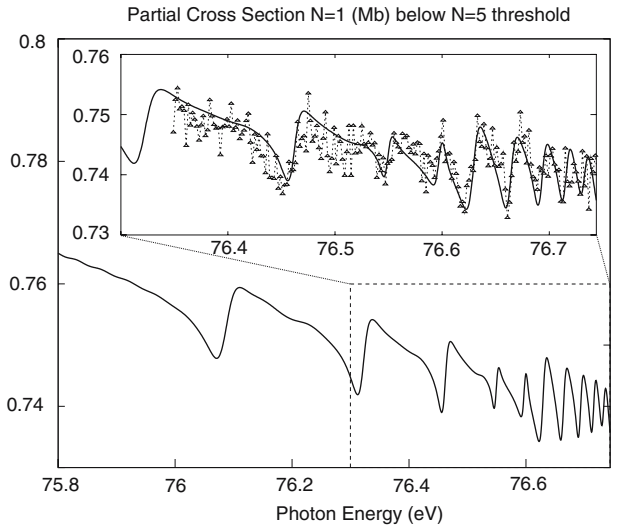

Fig. 5 Partial cross section σ_1 below $N = 5$ threshold. In the *inset* enlargement the present calculation (*continuous line*) is compared with data by Menzel et al. (*triangle*) [27]

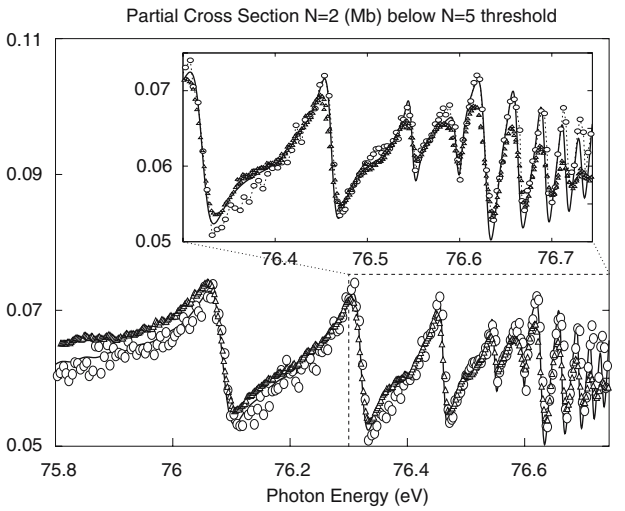

Fig. 6 Partial cross section σ_2 below $N = 5$ threshold. The present calculation (*continuous line*) is compared with data by Menzel et al. *triangle* [27] and by Jiang et al. *opencircles* [28]

slightly smaller. Very good agreement is found with Jiang data even for the height of the narrowest peaks.

Asymmetry parameters. In the dipole approximation, the angular distribution of electrons emitted in the photoionization of an orientationally averaged system by a linearly polarized incident light may be described by means of a single asymmetry parameter β [29]

$$\frac{\mathrm{d}\sigma}{\mathrm{d}\Omega} = \frac{\sigma}{4\pi}\left[1 + \beta\ (3\cos^2\theta - 1)/2\right] \tag{4}$$

where θ is the angle between the momentum of the ejected electron and the light polarization axis. Expressions like (4)

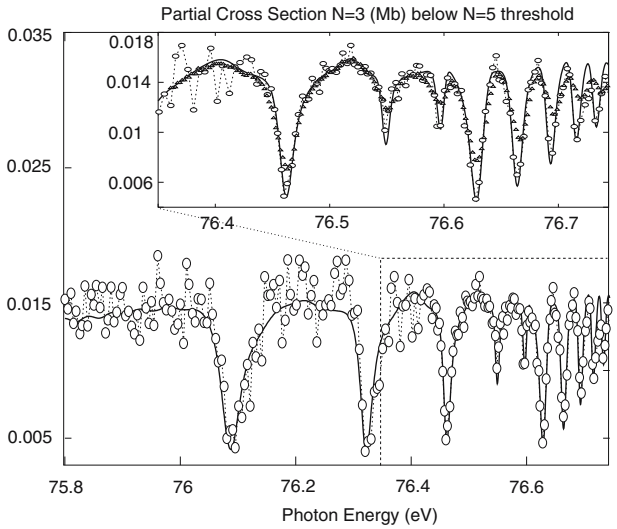

Fig. 7 Partial cross section σ_3 below $N = 5$ threshold (see Fig. 6)

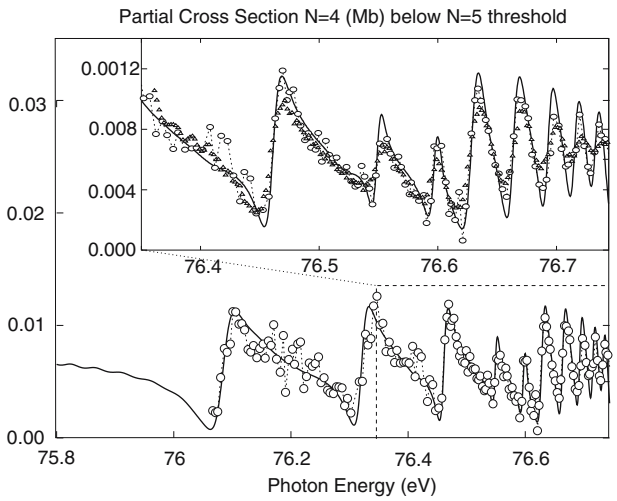

Fig. 8 Partial cross section σ_4 below $N = 5$ threshold (see Fig. 6)

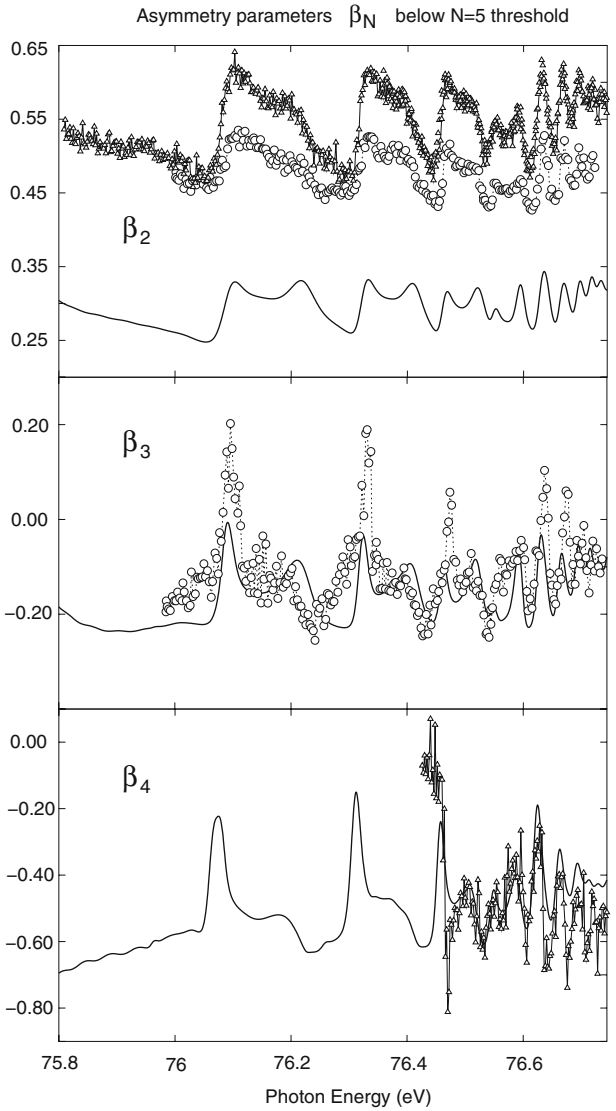

Fig. 9 Asymmetry parameters below $N = 5$ threshold (see Fig. 6)

hold for partial and total cross sections $\sigma_{N\ell}$, σ_N and $\sigma_{\rm tot}$ with weighted asymmetry parameters β_N:

$$\beta_N = \sum_\ell \sigma_{N\ell}\beta_{N\ell}/\sigma_N, \qquad \beta_{\rm tot} = \sum_N \sigma_N \beta_N/\sigma$$

It is well known that the calculation and measurement of the beta parameters are much more demanding than that of partial cross sections. In Fig. 9 the β_N parameters, convoluted with a 12 meV FWHM gaussian, are compared with experimental data by Menzel et al. [27] and Jiang et al. [28]. There is a good agreement in the resonant features of all plots. The largest disagreement between the two experiments ($\Delta\beta_2 \simeq 0.1$) and between theory and experiment ($\Delta\beta_2 \simeq 0.25$) is found for β_2. The data of Menzel are actually much more pronounced also in resonant features so that, by chance, they are reproduced with good approximations by twice our theoretical prediction. The absolute agreement is good in β_3 with Jiang data and in β_4 with Menzel data (Fig. 10).

4 Energy interval between $N = 5$ and 6 thresholds

Resonances. Below $N = 6$ threshold complete multiplets have 11 resonances each, which should be found in an energy interval correspondent to $\Delta n^* = 1$ (e.g. $\Delta E \simeq 45$ meV for $n^* = 8$). Considering that among so many resonances, some terms, mainly in $[131]^+$, $[221]^+$ and $[041]^+$ series, have widths comparable to the whole span of the corresponding multiplet, it is no surprise that it is quite difficult to characterize them with the fitting method. It is nevertheless possible to compare the density of states determined numerically with the same quantity reconstructed from resonance

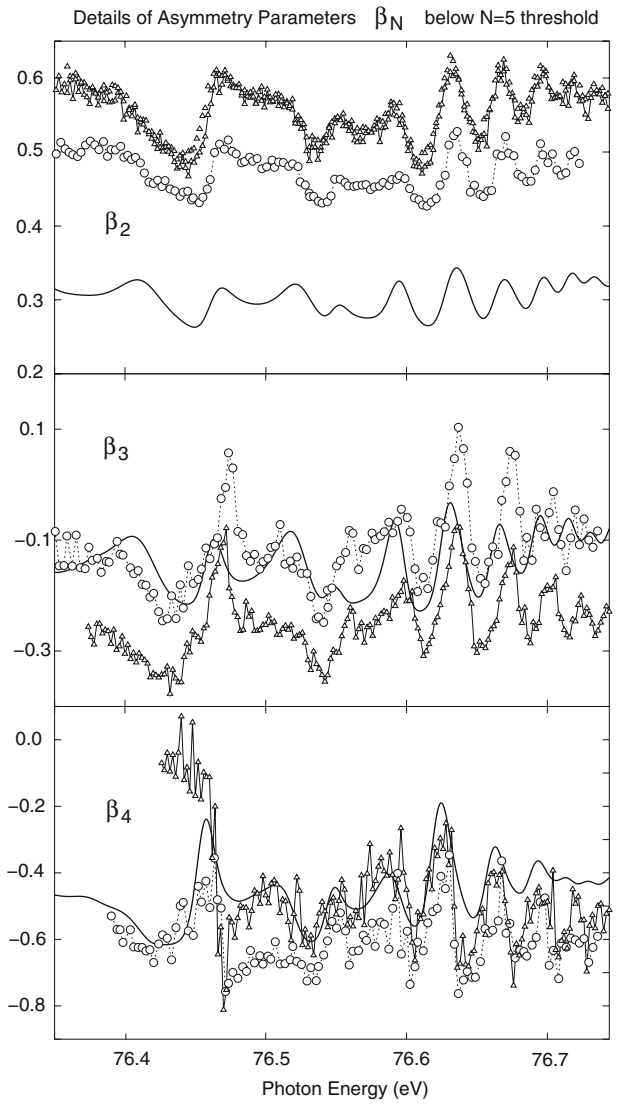

Fig. 10 Details of asymmetry parameters below $N = 5$ threshold (see Fig. 6)

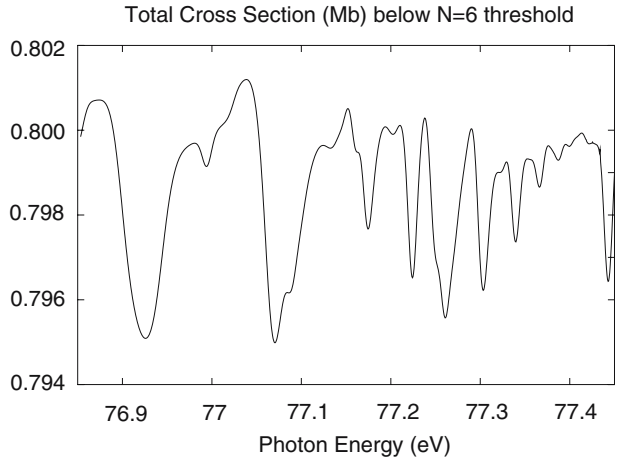

Fig. 11 Total cross section below $N = 6$ threshold with a linear background eliminated

parameters found in [7]. Even though a rather clear correspondance can be seen for many peaks, particularly those belonging to $[401]^+$, $[500]^-$, $[311]^+$ and $[320]^-$ series, the other assignments are more arbitrary. Differences are numerous and might be due to a bad representation of the intruder states from higher thresholds.

Cross sections. For cross sections, the agreement with available data is better than for resonances: here minor peaks in the theoretical predictions are not found in the experimental picture, but all main features are reasonably reproduced. In Figs. 11 and 12 total and partial cross sections are reported. Partial cross sections σ_2, σ_3, σ_4 and σ_5 are compared with the experimental results by Jiang et al. [28]. The theoretical results are convoluted with 10 meV (σ_{tot}) and 6 meV (σ_N) FWHM gaussian for a ready comparison with the cited experimental literature. In Fig. 11 a linear background $\sigma_{bg} = -(E - 77.1\,\text{eV}) \cdot .034\,\text{Mb/eV}$ has been subtracted to the total cross section for a clearer comparison with data by Domke et al. [22]. Experimental $\sigma_{2,3,4}$ have been shifted by 15 meV at lower energies for a closer comparison with our theoretical prediction. The two dominant peaks at 76.9 and 77.05 eV as well as the first four peaks in the group between 77.13 and 77.4 eV show a good correspondence. The last peaks are instead progressively more shifted to higher energies with a disagreement in the position of the last cumulative peak of roughly 15 meV. A problem of energy scale convention might be the origin of this discrepancy. More accurate theoretical results will be worth the effort of further investigation on this point, the present agreement being otherwise coherent with the overall numerical and experimental uncertainties. Experimental σ_5 data are available in the energy window between 77.15 eV and $N = 6$ threshold. With an energy shift of 8 meV downward, a remarkable agreement between several of the higher energy peaks is obtained.

Asymmetry parameters. As far as we know, theoretical partial cross section asymmetry parameters below $N = 6$ threshold have not yet been published and their experimental measurements appeared only in Jiang PhD dissertation (freely available online [10]). In Fig. 13 our theoretical predictions are compared with the existing measurements. β agreement is pretty good and some resonant features are clearly recognizable. Experimental β_2 data lies between 0.41 and 0.51 while our theoretical prediction lies between 0.46 and 0.54 which results in a relatively small average difference of 0.04. A clear correspondence between peak at 77.0 eV, valley at 77.08 eV and peak at 77.15 eV can be seen. Experimental and theoretical β_3 differ on average by ~ 0.1 units, and there are still correspondences analogous to those observed in β_2. It should be noted that modulations in theoretical and

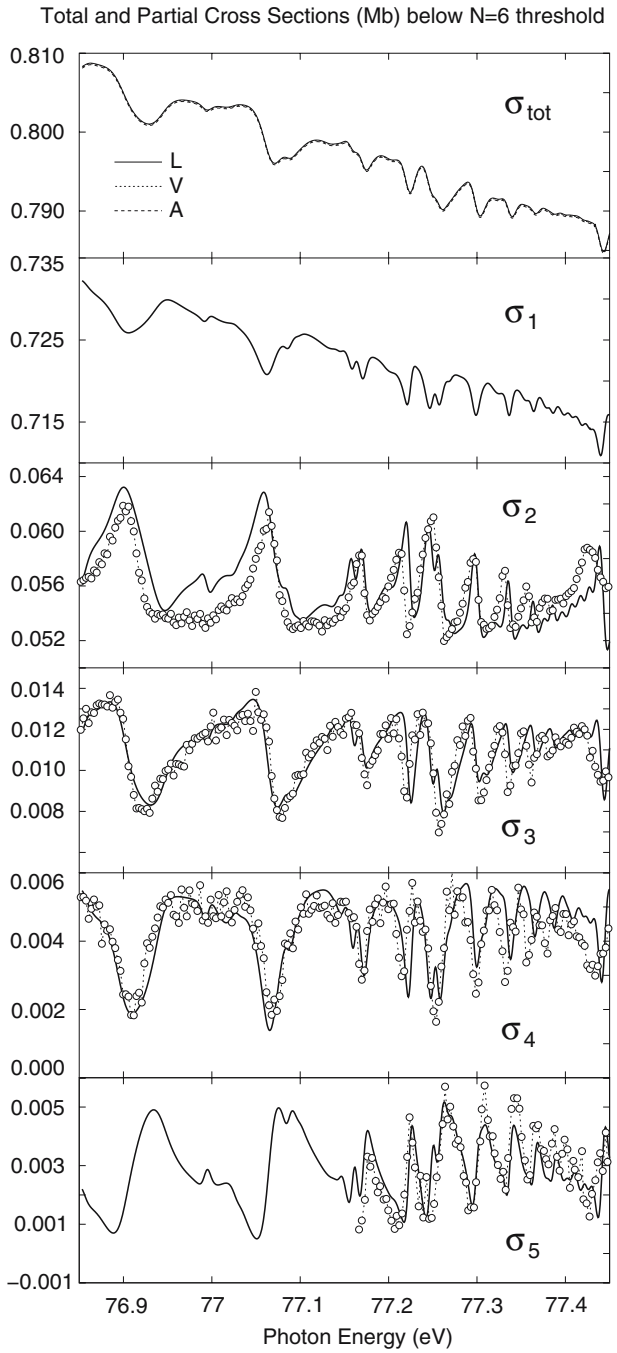

Fig. 12 Total and partial cross sections below $N = 6$ threshold. Comparison is made with experimental results (*opencircles*) by Jiang et al. [28] where available

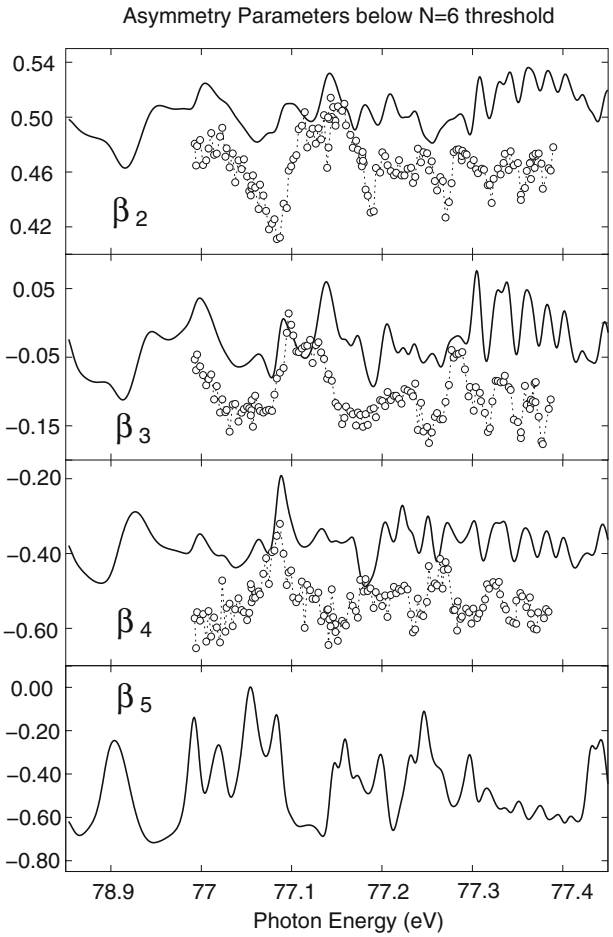

Fig. 13 Partial cross section asymmetry parameters β_N below $N = 6$ threshold. Experimental data *opencircles* are taken from Jiang PhD dissertation

experimental quantity are of comparable amplitude. In β_4 a difference of ~ 0.15 units between theory and experiment is found. A steep peak at ~ 77.08 eV is the most remarkable feature common to both experimental and theoretical data. Other correspondences are difficult to ascertain. For β_5 there are no experimental data at all. By the preceding comparisons it is safe to say that the present prediction of β_5 should reproduce the most prominent features of a possible experiment.

5 Conclusions

The K-matrix method using splines as elementary basis functions has been performed to calculate the photoionization spectrum of He in the energy intervals between $N = 4$ and 5 and between $N = 5$ and 6 ionization thresholds.

Below $N = 5$ threshold, the method, as it stands, yields accurate resonance parameters, partial cross sections σ_N and asymmetry parameters β_N, while in the second interval the determination of the resonance parameters shows some inadequacy. σ_N nevertheless appear to be pretty good and compare well with the available theoretical and experimental data. Also the β_N's, which, as far as we know, have been computed for the first time, compare favorably with some very recent preliminary experimental results kindly supplied to us by Jiang and still unpublished.

Acknowledgements We are grateful to Dr. Alexander Menzel for providing us with experimental data below $N = 5$ threshold and Dr. Yuhai Jiang for providing us with experimental data some of which are still unpublished.

References

1. Madden RP, Codling K (1963) Phys Rev Lett 10:516
2. Fano U, Cooper JW (1965) Phys Rev 137:A1364
3. Püttner R, Domke M, Gremaud B, Martins M, Schlachter AS, Kaindl G (1999) J Electron Spectros 101–103:27
4. Jiang YH, Püttner R, Hentges R, Viefhaus J, Poygin M, Cacho C, Becker U, Rost JM, Kaindl G (2006) J Phys B At Mol Opt Phys 39:L9
5. van der Hart HW, Greene CH (2002) Phys Rev A 66:022710
6. Schneider T, Liu CN, Rost JM (2002) Phys Rev A 65:042715
7. Rost JM, Schulz K, Domke M, Kaindl G (1997) J Phys B At Mol Opt Phys 30:4663
8. Püttner R, Grémaud B, Delande D, Domke M, Martins M, Schlachter AS, Kaindl G (2001) Phys Rev Lett 86:3747
9. Argenti L, Moccia R (2006) J Phys B At Mol Opt Phys 39:2773
10. Jiang Y (2006) Doubly excited helium: from strong correlation to chaos. http://www.diss.fu-berlin.de/2006/269
11. Cacelli I, Carravetta V, Moccia R (1986) J Chem Phys 85:7038
12. Cacelli I, Carravetta V, Rizzo A, Moccia R (1991) Phys Rep 205:283
13. Moccia R, Spizzo P (1991) Phys Rev A 43:2199
14. Mengali S, Moccia R (1996) J Phys B At Mol Opt Phys 29:1597
15. Fang TK, Chang TN (2000) Phys Rev A 61:062704
16. Jiang Y, Yan J, Li J, Sun J, Wan L (2000) Phys Rev A 61:032721
17. Tang JZ, Shimamura I (1994) Phys Rev A 50:1321
18. Freund DE, Huxtable BD, Morgan JD III (1984) Phys Rev A 29:980
19. Carroll DP, Silverstone HJ, Metzger RM (1979) J Chem Phys 71:4142
20. Woodruff PR, Samson JAR (1982) Phys Rev A 25:848
21. Domke M, Xue C, Puschmann A, Mandel T, Hudson E, Shirley DA, Kaindl G, Greene CH, Sadeghpour HR, Petersen H (1991) Phys Rev Lett 66:1306
22. Domke M, Schulz K, Remmers G, Gutiérrez A, Kaindl G, Wintgen D (1995) Phys Rev A 51:R4309
23. Menzel A, Frigo SP, Whitfield SB, Caldwell CD, Krause MO, Tang JZ, Shimamura I (1995) Phys Rev Lett 75:1479
24. Zubek M, King GC, Rutter PM, Read FH (1989) J Phys B At Mol Opt Phys 22:3411
25. Zubek M, Dawber G, Hall RI, Avaldi L, Ellis K, King GC (1991) J Phys B At Mol Opt Phys 24:L337
26. Sokell E, Wills AA, Comer J, Hammond P (1996) J Phys B At Mol Opt Phys 29:L83
27. Menzel A, Frigo SP, Whitfield SB, Caldwell CD, Krause MO (1996) Phys Rev A 54:2080
28. Jiang YH, Püttner R, Hentges R, Viefhaus J, Poiguine M, Becker U, Rost JM, Kaindl G (2004) Phys Rev A 69:042706
29. Huang KN (1980) Phys Rev A 22:223